Mon. Not. R. Astron. Soc. **000**, 000–000 (0000) Printed 9 December 1999 (MN LATEX style file v1.4)

The tilt of the Fundamental Plane of Early-type galaxies: wavelength dependence. ⋆

M. Scodeggio,[1] G. Gavazzi,[2]† E. Belsole,[2] D. Pierini,[3] A. Boselli[4]
[1] *European Southern Observatory, Karl-Schwarzschild-Str. 2, D-85748 Garching bei München, Germany*
[2] *Università degli Studi di Milano, dipartimento di Fisica, via Celoria 16, 20133 Milano, Italy*
[3] *Max-Planck-Institut für Kernphysik, Postfach 103980, D-69117 Heidelberg, Germany*
[4] *Laboratoire d' Astronomie Spatiale BP8, Traverse du Syphon, F-13376 Marseille, France*

ABSTRACT
The photometric parameters R_e and μ_e of 74 early-type (E+S0+S0a) galaxies within 2 degrees projected radius from the Coma cluster centre are derived for the first time in the near IR H band (1.65 μm). These are used, coupled with measurements of the central velocity dispersion σ found in the literature, to determine the H band Fundamental Plane (FP) relation of this cluster: log $R_e \propto A\ log\ \sigma + b\ \mu_e$. The same procedure is applied to previously available photometric data in the B, V, r, I, and K bands, to perform a multi-wavelength study of the FP relation. Because systematic uncertainties in the value of the FP parameters are introduced both by the choice of the fitting algorithm used to derive the FP template, and by the presence of statistical biases connected with the sample selection procedure, we emphasize the importance of deriving the FP parameters in the six different photometric bands using an identical fitting algorithm, and appropriate corrections to eliminate the effects of sample incompleteness. Once these corrections are applied, we find that the FP b coefficient is stable with wavelength ($\sim 0.35\ \pm 0.02$), while the A coefficient increases significantly with increasing wavelength: from $\sim$1.35 to $\sim$ 1.70 ($\pm$0.1) from the optical to the IR, in agreement with an earlier result presented by Pahre & Djorgovski (1997). Therefore the slope of the FP relation, although changing with wavelength, never approaches the virial theorem expectation (A=2.0) when the central velocity dispersion only is used to build the FP. We also find that the magnitude of the slope change can be entirely explained by the presence of the well known relation between color and magnitude among early-type galaxies. We conclude that the tilt of the Fundamental Plane is significant, and must be due to some form of broken homology among early-type galaxies, while its wavelength dependence derives from whatever mechanism (currently the preferred one is the existence of a mass-metal content sequence) produces the color-magnitude relation in those galaxies.

Key words: Galaxies: elliptical and lenticular, cD – Galaxies: fundamental parameters – Galaxies: stellar content – Galaxies: clusters: individual: Coma.

1 INTRODUCTION

Elliptical galaxies populate a two-dimensional manifold in the space of their observable properties. This is generally defined in terms of the galaxy effective radius r_e (the radius that contains half of the galaxy total light), effective surface brightness μ_e (mean surface brightness within the effective radius) and central velocity dispersion σ, and has been named the Fundamental Plane (FP) (Djorgovski & Davis 1987, Dressler et al. 1987). Alternative representations of this manifold are also possible, and were obtained substituting σ with broad-band colors (de Carvalho & Djorgovski 1989), or relative luminosities (Scodeggio et al. 1997b). The very existence of the FP has profound implications for the processes that led to the formation and evolution of elliptical galaxies (see for example Guzmàn et al. 1993, Pahre & Djorgovski 1997, Graham & Colless 1997a; Burstein et al. 1997). In particular its tightness provides a very strong con-

⋆ Based on observations taken at TIRGO (Gornergrat, Switzerland). TIRGO is operated by CAISMI-CNR, Arcetri, Firenze, Italy.
† Osservatorio Astronomico di Brera, via Brera 28, 20121, Milano, Italy

straint on the evolutionary history of those systems. At the same time, this tightness makes the FP a powerful tool for deriving redshift independent distance estimates, that can be obtained with uncertainties of about 15-20 per cent for a single galaxy.

If elliptical galaxies had perfectly homologous structural and kinematic properties (their kinematic and density profiles were identical), then the Virial theorem would predict the FP to have the form $r_e \sim \sigma^2 * \Sigma_e^{-1} (M/L)^{-1}$, where M/L is the galaxy mass to light ratio. Under the assumption of a constant M/L, the observed FP should then be log $r_e \sim 2 \; log \; \sigma + 0.4 \; \mu_e$. In practice, however, the log σ and μ_e coefficients have been determined to lie in the range 1.2–1.6, and 0.30–0.35, respectively. The difference between the expectation and the observed parameters of the FP is generally named 'tilt' of the FP. This tilt is usually viewed as the product of systematic variations of M/L along the FP, that can be parameterized as M/L $\sim L^{\beta}$. The parameter β is connected to the log σ coefficient A by the relation $\beta =$ (2-A)/(2+A) (Pahre et al. 1995). Among the possible explanations that have been considered for the tilt, there are variations in the stellar population along the FP, due to possible variations in age, metallicity, or initial mass function (Djorgovski & Santiago 1993, Renzini & Ciotti 1993, Pahre et al. 1995, Pahre & Djorgovski 1997), changes in the dark matter content (Renzini & Ciotti 1993), and deviations from homology, both in the kinematical structure (Capelato et al. 1995) and in the matter (and light) distribution (Hjorth & Madsen 1995, Ciotti et al. 1996, Graham & Colless 1997a). Observationally, the possibility of distinguishing between changes in the stellar population and broken homology is linked to the wavelength dependence of the tilt produced by the stellar population effects, compared with a tilt that should be strictly independent of wavelength if produced by broken homology.

Claims of a detection of systematic changes of the tilt with wavelength have been presented, but the situation is still uncertain. A quick and certainly incomplete survey of the FP parameters derived by different authors during this last decade is presented in Table 1, and illustrates well this uncertainty. The main source of confusion about the possible wavelength dependence of the FP tilt is in the way comparisons between several wavelengths have been performed, that is simply comparing fits obtained by various groups, that had used different samples, and different fitting algorithms to derive the FP parameters. Both these differences can significantly affect the comparison, artificially producing different FP relations in various photometric bands.

First, systematic uncertainties introduced by the choice of a given fitting algorithm in the derivation of the FP are most likely the dominant source of uncertainty in the value of the FP parameters. Different algorithms applied to the same sample can produce values of the log σ coefficient, and therefore of the tilt, that differ from each other by up to 25 per cent (the value of the μ_e coefficient is a lot more stable, see section 5). Therefore, since there is no well established fitting technique for FP data-sets, it is most dangerous to compare results from different works. Second, sample selection biases have been generally ignored in the derivation of FP templates. The most important bias for FP works, that are generally based on samples of galaxies taken from rich clusters of galaxies, is the so-called cluster population incompleteness bias (Teerikorpi 1987, 1990; Sandage 1994a,b). Because of the systematic lack of faint galaxies in observed samples, a biased FP relation is obtained by simply fitting a plane to such samples. This bias manifests itself as a flatter slope and a reduced scatter in the observed FP, with respect to the true, unbiased one. The amount of bias introduced in the observed FP depends on the completeness of the sample, and therefore various FP relations, obtained from different samples, can suffer from varying biases, and therefore appear to have different tilt.

Although without addressing these possible problems, Pahre & Djorgovski (1997) were the first to derive firm evidence of a wavelength dependence of the FP parameters. Comparing the FP relation they obtained using K band photometric parameters with the one obtained by Lucey et al. (1991) using V band data, they concluded that the K band FP relation differs both from the optical one, and from the virial expectation. Their result was reproduced by Mobasher et al. (1997), also using K band photometric data.

With the aim of better determining the wavelength dependence of the tilt of the FP, we present here a multi-band FP study, based on galaxies belonging to the Coma cluster. The choice of this cluster is guided by two main reasons: 1) the FP relation in this cluster is known to have a small scatter (see e.g. Jorgensen et al. 1996: Scodeggio et al. 1997a); 2) a large body of photometric and spectroscopic data is available for this cluster. We supplement the existing photometric data with a newly obtained set of NIR H band (1.65 μm) observations, obtained as part of a large near-IR imaging survey of all early type (E+S0+S0a) galaxies in the Coma Supercluster. Including these new data, we have now available photometric measurements for at least 30 galaxies (that also have spectroscopic measurements available) in 6 different bands: B, V, r, I, H, and K. The FP parameters in these bands are determined using a unique fitting algorithm, therefore eliminating the most important source of uncertainty in the differential comparisons between bands, and the results are corrected for the effects of sample incompleteness using a set of Monte Carlo simulations, a technique pioneered by Giovanelli et al. (1997) for Tully-Fisher work, and applied to the FP by Scodeggio et al. (1997a).

The remaining of this paper is organized as follows: in section 2 we discuss the sample of galaxies used in this work; in section 3 we present the new H band observations of 74 early-type galaxies in Coma, in section 4 the total data-set used in this work, and in section 5 the derivation of the FP relation in the 6 different photometric bands; the concluding discussion is presented in section 6.

2 THE SAMPLE

The galaxies analysed in this work are selected from the CGCG catalogue (Zwicky et al. 1961-68) ($m_p \lesssim 15.7$), within a 2.0 degrees radius from the X ray centre of the Coma cluster ($\alpha = 12^h 57^m 30^s$, $\delta = 28°15'00''$). There are 139 such objects with morphological classification E, S0, S0a. Among these we reject those objects whose membership to the cluster is uncertain due to either too large a velocity discrepancy for their angular separation (see Gavazzi et al. 1995) or because they belong to the NE filament departing from the Coma cluster (Gavazzi 1987), whose distance could differ from that of Coma. Among the remaining objects we chose all those with available measurements of the central velocity dispersion (Davies et al. 1987, Dressler 1987, Faber et al. 1989, Lucey et al. 1991b, Scodeggio et al. 1997a), for a total of 79 objects.

For those objects we searched in the literature for measurements of the photometric parameters used in FP studies. We have found data for 42 galaxies in the B band (Burstein et al. 1987; Faber et al. 1989; Saglia et al. 1993a; Prugniel & Simien, 1996), 42 in V (Lucey et al. 1991b), 55 in r (Jorgensen et al. 1995), 79 in I (Scodeggio et al. 1997a, 1998a), 29 in K (Mobasher et al. 1997). To those we add here measurements for 74 galaxies in the H band. All galaxies are assumed to be at a distance of 96 Mpc (μ_o=34.91), derived from a mean cluster heliocentric recessional velocity of 6917 km s^{-1}, corrected to 7185 km s^{-1} to account for the motion with respect to the Cosmic Microwave Background (Kogut et al. 1993), and assuming H$_o$ = 75 km s^{-1}Mpc^{-1}.

3 H BAND OBSERVATIONS AND DATA REDUCTION

The H band observations of 74 galaxies presented in this work are part of an extensive survey of all early type galaxies with $m_p < 15.7$ in the Coma Supercluster region $11^h30^m < \alpha < 13^h30^m$; $18° < \delta < 32°$. The entire survey will be described elsewhere (Gavazzi et al. in preparation). The observations were carried out with the TIRGO 1.5 m telescope at Gornergrat equipped with the NICMOS3 camera "ARNICA" (Lisi et al. 1993, 1995) in 22 nights from March 13 to April 13, 1997. The optical setting of the camera provides a field of view of 4.3 arcmin^2 with 0.96 arcsec pixels. The average seeing was 2.3 arcsec. The observing technique was similar to that used in previous observations of late-type galaxies, as described in Gavazzi et al. (1996). Here we briefly summarize some of the observing parameters relevant to this work. All galaxies with apparent B diameter > 1.0 arcmin were observed with pointing sequences which consist of eight frames centered on the source, alternated with eight sky frames, positioned along a circular path around the source and offset by 4 arcmin. The on-source positions were dithered by 10 arcsec to improve the flat-fielding, and to facilitate the bad pixel removal. The total integration time was 6.4 min, both for the target galaxy and for the sky frames. Galaxies with apparent B diameter < 1.0 arcmin were observed with sequences of 9 pointings along a circular path, displaced from one-another by 1 arcmin, such that the target galaxy was always in the field. The total integration time was 7.2 min. To check the consistency of the photometric calibration, 26 galaxies were observed twice or more times during different nights. For those objects we report here the measurements obtained on the combined frames. The data were calibrated with standard stars in the Elias et al. (1982) catalogue, with a typical photometric uncertainty of 0.05 mag.

The basic image reduction was performed using standard routines in the IRAF‡-STSDAS§-PROS environment. The bias-subtracted, flat-fielded, combined, and calibrated images were analysed using the package GAPLHOT (developed for IRAF-STSDAS mainly by W. Freudling, J. Salzer, and M. Haynes, and adapted by one of us (M.S.) to perform the light decomposition of early-type galaxies). For each frame the sky background was determined as the mean number of counts measured in regions of "empty" sky, and it was subtracted from the frame. Sky-subtracted frames were inspected individually and the light of unwanted superposed or nearby stars and galaxies was masked. The 2-dimensional light distribution of each galaxy was fitted with elliptical isophotes, using a modified version of the STSDAS *isophote* package. The fit maintains as free parameters the ellipse centre, ellipticity and position angle, and the ellipse semi-major axis is incremented by a fixed fraction of its value at each step of the fitting procedure. Using the fitted parameters a model of the galaxy light distribution is obtained, which is used to compute integrated magnitudes as a function of semi-major axis. As an example, we show in Fig.1 the calibrated frame of NGC 4889 prior and after subtraction of the model fitting.

The effective radius r_e and effective surface brightness μ_e (the mean surface brightness within r_e) of each galaxy were obtained by fitting its radial surface brightness profile with a de Vaucouleurs $r^{1/4}$ law (de Vaucouleurs 1948). The fit was performed from a radius equal to twice the seeing radius, out to the outermost isophotes for E galaxies; for S0 and S0a galaxies only the central core was fitted. The median uncertainty on the determination of log r_e and μ_e is 0.05 and 0.16 mag., respectively. Total magnitudes were obtained by extrapolating the $r^{1/4}$ fit to infinity (E galaxies), or by extrapolating to infinity the exponential profile that fitted the outer parts of the galaxy light profile (S0 and S0a galaxies), and adding the flux corresponding to the extrapolated part of the profile to the one measured within the outermost fitted galaxy isophote. The median uncertainty in the determination of the total magnitude is 0.15 mag.

The derived parameters are listed in Table 2 as follows:
Column 1: CGCG designation (CGCG field and ordinal number within that field).
Columns 2-4: effective radius, observed and corrected for seeing according to the prescriptions of Saglia et al. (1993b), with uncertainty (in arcsec).
Columns 5-6: logarithm of the effective metric (corrected) radius in kpc, with error.
Columns 7-9: effective surface brightness, observed and corrected, with uncertainty (in magnitudes per square arcsec). The correction includes the cosmological expansion $(1+z)^4$ and K-correction (taken to be proportional to 1+z) terms, and the seeing correction, according to Saglia et al. (1993b). No galactic absorption correction was applied since A$_H$ = 0.085 A$_B$ (Pahre et al. 1996), with A$_B$ $\sim$ 0.1 mag

‡ IRAF (Image Reduction and Analysis Facility) is distributed by NOAO, which is operated by the Association of Universities for Research in Astronomy, Inc. (AURA), under cooperative agreement with the National Science Foundation.

§ STSDAS(Space Telescope Science Data Analysis System) is distributed by STScI, which is operated by AURA, under contract to the National Aeronautics and Space Administration.

in the direction of Coma.
Column 10: seeing (arcsec).

4 DERIVED PARAMETERS.

Table 3 lists the FP related parameters not already included in Table 2 for the 79 galaxies considered in this work. The table is arranged with two lines for each galaxies. On the first line the measured spectroscopic and photometric parameters are given, while on the second line there are the relative measurement uncertainties. The columns are as follows:
Columns 1-2: CGCG designation (CGCG field and ordinal number within that field), and NGC/IC number.
Column 3: morphological type, with reference.
Column 4: Recessional velocity corrected for the bulk motion with respect to the Cosmic Microwave Background.
Columns 5-6 : logarithm of the central velocity dispersion with associated uncertainty and reference. The velocity dispersion measurements were taken from the following sources: a) Scodeggio et al. (1997a) (19); b) Davies et al. (1987) (8); c) Lucey et al. (1991b) (28); g) Faber et al. (1989) (7); i) Dressler (1987) (17). Although these measurements were taken using somewhat different apertures (a used 2×6 arcsec apertures, c used 2×5.8 arcsec ones, i lists data corrected to 2×4 arcsec ones, b and g used 4×4 arcsec ones (LCO measurements); only one velocity dispersion in the present sample (for the galaxy 160070) was measured in a 1.5×4 arcsec aperture (Lick data)), they were shown to be in good relative agreement (Lucey et al. 1991b; Scodeggio 1997), with the exception of the measurements presented by Dressler (1987; see Davies et al. 1987, and Lucey et al. 1991b). To compensate for the measured offset in the velocity dispersion scale of the Dressler (1987) observations, we have applied to them a correction of 0.016 dex (Davies et al. 1987). The uncertainties associated to the velocity dispersion measurements are quoted individually in refs a and c. They are quoted 14 and 9 per cent, respectively, for the Lick and for the remaining observations in refs b and g. They are quoted 10 per cent in ref i.
Columns 7-9 : B band parameters: log R_e with error, μ_e with error, and reference. The references are: e: Saglia et al. (1993a) (29); h: Burstein et al. (1987) (1); g: Faber et al. (1989) (9), m: Prugniel & Simien, (1996) (3). The photometric parameters were derived by Saglia et al. (1993a) by fitting $r^{1/4}$ laws to the radial photometric profile derived from 2-D data. The μ_e are corrected for cosmological effects and for Galactic absorption. Both R_e and μ_e are corrected for seeing. Burstein et al. (1987) and Faber et al. (1989) derived effective circular diameters (A_e) and μ_e from a combination of photoelectric and CCD measurements. These data are corrected for cosmological effects and for Galactic absorption, but are not corrected for seeing. The uncertainties quoted by Saglia et al. (1993a) are 0.1 and 0.05 respectively on μ_e and log R_e. Burstein et al. (1987) and Faber et al. (1989) quote the uncertainties according to four quality-classes of their observations. The data from Prugniel & Simien, (1996) are corrected for cosmological effects and for Galactic absorption, but are not corrected for seeing. These authors give total magnitudes and μ_e. log R_e is derived using m_T=μ_e - 2.0 - 5log r_e
Columns 10-12 : Same as cols. 6-8 for V band. Measurements are taken from c: Lucey et al. (1991b) (42). The photometric parameters μ_e and R_e were derived by fitting $r^{1/4}$ laws to the radial photometric profile derived from 2-D data. The μ_e are corrected for cosmological effects, and Galactic absorption. Both μ_e and R_e are corrected for seeing. The uncertainties on μ_e and R_e are 0.14 mag and 0.028 dex respectively.
Columns 13-15 : Same as cols. 6-8 for r band. Measurements are taken from d: Jorgensen et al. (1995) (55). The photometric parameters μ_e and R_e were derived by fitting $r^{1/4}$ laws to the radial photometric profile derived from 2-D data. The μ_e are corrected for cosmological effects, and for Galactic absorption. Both μ_e and R_e are corrected for seeing according to the prescriptions of Saglia et al. (1993b). The uncertainties on μ_e and R_e are quoted by Jorgensen et al. (1995) for each individual galaxy.
Columns 16-18 : Same as cols. 7-9 for I band. Measurements are taken from a: Scodeggio et al. (1997a, 1998a) (79). The photometric parameters μ_e and R_e were derived by fitting $r^{1/4}$ laws to the radial photometric profile derived from 2-D data. The μ_e are corrected for cosmological effects, and for Galactic absorption. Both μ_e and R_e are corrected for seeing according to the prescriptions of Saglia et al. (1993b). The uncertainties on μ_e and R_e are given by the authors for each individual galaxy.
Columns 19-21 : Same as cols. 7-9 for K band. Measurements are taken from Mobasher et al. (1997) (29). The photometric parameters μ_e and R_e were derived on the integrated profiles (growth curves). Their r_e is the radius that contains half of the asymptotic magnitude and μ_e is the mean surface brightness within that radius. μ_e is corrected for cosmological effects, and for Galactic absorption. No seeing corrections were applied, but the observations were carried out in 1 arcsec seeing conditions and the corrections were estimated $\lesssim$ 0.01 dex by the authors. The authors quote that the uncertainties on μ_e and log R_e are 0.03 mag and 0.02 dex respectively.

The photometric parameters that enter in the FP determination (μ_e and R_e) obtained at the various wavelengths are plotted for comparison in Fig. 2a and b against the H band values. There is a general agreement between the various sets of measurements, except for the K band data, and for a few galaxies marked in the figures. The larger scatter shown by the comparison between the H band and the B, V, and r band data, with respect to the comparison between the H band and the I band data, is mainly due to different fitting techniques adopted in the case of galaxies that do not follow the $r^{1/4}$ relation at all radii (see Scodeggio et al. 1998a). The K band data have a markedly different distribution from those at any other band: both μ_e and R_e span half the range covered by the remaining measurements. When combined they produce a K band FP that extends considerably less than in other bands (see Fig. 5), and with a slope significantly different from the one derived by other authors at similar wavelengths (e.g. Pahre & Djorgovski 1997). The reason for this disagreement is unclear. The good correlation observed among the parameters derived at all other bands shows that strong colours gradients within the galaxies are to be excluded. Thus the discrepancy is probably a spurious result, that might derive from the fact that the method used by Mobasher et al. (1997) to determine the K band photometric parameters differs from that used in other bands (see above). In fact these parameters were derived from the integral growth curves, instead of from the surface brightness profiles. Further support to this conclusion is given by the presence of simultaneous discrepancies in μ_e and r_e: the galaxies with large r_e appear to be both too bright and too small in the K band data. Due to the known anti-correlation between μ_e and r_e (depending on the details of the light profile, a small r_e coupled with a bright μ_e or a larger r_e with a fainter μ_e produce similarly acceptable fits), however, individual discrepancies on r_e or μ_e do not necessarily reflect in large deviations on the FP. This is shown in Fig. 2c, where the values measured in different photometric bands for the combination of μ_e and r_e that enters in the FP are compared. The good correlation between the H band data and those in all other bands, including K, is clearly visible.

5 THE FP RELATION IN DIFFERENT PHOTOMETRIC BANDS

5.1 Fitting the FP parameters

Finding the best-fit FP parameters is a non trivial statistical exercise. The fitting algorithm must minimize the 'distance' of a set of points (x,y,z) with associated uncertainties (ϵx, ϵy, ϵz) from a plane $z = a + bx + cy$, taking into account that the uncertainties are not statistically independent quantities. Here we fit the FP by minimizing the weighted sum of the orthogonal distances of the data points from the plane. This is a generalization to 3 dimensions of the maximum likelihood method of Press et al. (1992) (their "fitexy" routine), with a modification introduced to take into account the high degree of covariance shown by the uncertainties on the determination of log R_e and μ_e (see Scodeggio 1997, and Scodeggio et al. 1998b for details). Uncertainties on the FP parameters are determined using the statistical jackknife: N sub-samples, each one composed of N–1 data-points, are extracted from the original sample of N data-points, rejecting in turn one of the data-points. The distribution of a certain statistical parameter among those N sub-samples is then used to estimate the uncertainty in the value of that same parameter, without having to assume an a-priori statistical distribution for the parent population of the data-set under examination (see for example Tukey 1958, and Efron 1987).

5.2 Completeness corrections

The heterogeneous nature of the photometric samples used in this work results into FP samples that have significantly different completeness. This fact must be taken into account, before a meaningful comparison of the FP parameters obtained at different photometric bands can be made. Cluster samples used for the determination of distance-indicator relations like the FP or the Tully-Fisher relation suffer from an important statistical bias, usually called cluster population incompleteness bias (Teerikorpi 1987, 1990). Because of the systematic lack of faint cluster members in a realistic sample, a bias is introduced in the determination of the relation parameters: the 'slope' and the scatter of the relation are underestimated, and, as a consequence, the relation zero-point is overestimated (see Sandage 1994a, b for a detailed analysis of this effects). The amount of bias introduced is clearly dependent on the degree of completeness of the sample. Since here we are interested in the relative values of the FP parameters in different photometric bands, one solution to the completeness problem would be to limit our analysis to a subset of objects that have photometric observations at all bands, so that the sample completeness would be the same at all bands. This approach would however reduce significantly the size of the available samples, and therefore significantly increase the uncertainty in the determination of the FP parameters. For this reason we prefer to use the full sample at all bands, and correct the FP parameters for the effects of sample incompleteness.

The estimate of the sample completeness is obtained as follows: we first model the B band luminosity function (LF) of (giant) early-type galaxies as a Gaussian (Sandage et al. 1985). The peak of the Gaussian is assumed to be at $B_{peak} = 16.75$, which corresponds to $B_{peak} = 13.0$ derived by Sandage at al. (1985) in Virgo, assuming a differential distance modulus (Coma-Virgo) of 3.75 mag (see, for example, the recent compilation by D'Onofrio et al. 1997). The width of the Gaussian that better fits our total sample of CGCG galaxies is however significantly lower than the Sandage et al. value, as shown in Fig. 3. We find $\sigma = 1.1$, in good agreement with Scodeggio et al. (1997b), who determined the LF of early-type galaxies using a composite sample of galaxies from 3 different clusters, and also in agreement with the determination of the bright end of the Coma cluster LF obtained by Thompson & Gregory (1993), and by Biviano et al. (1995). We then assume that this LF provides a good description of the early-type galaxies LF at all bands. This is equivalent to assuming a constant color term to perform the transformation from B to VrIHK, neglecting the small differences introduced by the color-magnitude relation. This approximation is justified here, since it does introduce only negligible effects in the computation of the FP completeness corrections. The solid histograms in Fig. 3 give the B mag distribution of galaxies that enter in the FP study, binned in 0.4 mag intervals, for the samples that have available σ measurements, and R_e and μ_e measurements in the BVrIHK bands, respectively. The dashed-line histogram is the total CGCG sample, and the dot-dashed line is the best fitting Gaussian LF. The ratio of the number of galaxies in the FP sample to that expected from the Gaussian LF in the same bin gives the sample completeness as a function of B mag (see histograms in Fig. 3). Finally, the characteristic magnitude B_{compl} and cut-off slope are obtained fitting a Fermi–Dirac function to the completeness distribution in the 6 observed bands (solid line curves in Fig. 4). The Fermi-Dirac parameters so derived are listed in Tab. 4.

More than one analytical treatment has been presented on the derivation of sample incompleteness bias corrections for distance-indicator relations (see Willick 1994, Sandage 1994a, b; Sandage e al. 1995). Magnitudes however enter only indirectly into the FP diagram, via the L-R_e, L-σ and L-μ_e relations. The systematic lack of fainter galaxies, at any given σ or μ_e, reflects only marginally into a lack of small R_e objects. It is thus impossible to convert directly the magnitude completeness of a sample into a R_e, σ or μ_e completeness. Moreover, all the analytical treatments assume that one is dealing with strictly magnitude limited samples, which is almost never the case, and certainly it is not with our samples. For these two reasons we then use Monte Carlo simulations to derive incompleteness corrections. This technique was pioneered by Giovanelli et al. (1997) for Tully-Fisher work, and applied to the FP by Scodeggio et al. (1997a).

The simulations are used to reproduce the observed relations between the galaxy luminosity and the parameters R_e, μ_e, and σ, and the relation between R_e and μ_e (Kormendy 1977). By then selectively removing from the simulations the fainter galaxies, it is possible to reproduce the effect of luminosity incompleteness on the FP parameters (see Scodeggio 1997 for details). Because of the lack of low luminosity objects, R_e is on the average overestimated in incomplete samples, except at the bright end of the sample. This results in a shallower slope of the FP compared with the corrected slope. Here the corrections were determined using an iterative procedure, where the simulation input parameters, representing the 'true' FP relation that would be observed with a complete sample, were adjusted until the output of the simulation, given certain completeness parameters, reproduced the observed FP relation, as obtained with the incomplete sample. At this point, the input parameters were taken to be those of the correct FP relation.

5.3 Results

The FP relation at different wavelengths was derived using the samples listed in Table 2 and 3, and the fitting method described in section 5.1. A 2.5 σ clipping criterion was applied during the fitting procedure: after a first fit was obtained, objects that deviated from the best-fit plane by more than 2.5 times the measured dispersion were removed from the sample, and a second fit was obtained. No second iteration of this procedure was necessary. The resulting FP parameters are listed in Tab. 5 together with the number of galaxies used in the fit. An edge-on view of the FP in the various bands is given in Fig. 5 (left panels), where the solid line represents the projection of the best-fit relation. A clear trend in the value of the log σ coefficient with wavelength is present, but this could be partly due to the varying degree of completeness of the samples used in the fit, with the I, and H band samples being significantly more complete than the B, V, and r band ones. The parameters listed in Tab. 5, together with the completeness parameters listed in Tab. 4, were used in the Monte Carlo simulations to derive completeness-corrected FP relations at the various wavelengths. The parameters for these corrected relations are given in Tab. 6. Statistical uncertainties on these parameters were obtained adding the uncertainties from the original fits, listed in Tab. 5, to the statistical uncertainties with which the simulations reproduce those fits. Also, these new, completeness-corrected FP relations are shown in the right panels of Fig. 5 (note that the data-points plotted are still the same as in the left panels). The completeness corrections increase the σ coefficients by about 0.2 on average, while the μ_e coefficients are very little changed. The exact magnitude of the correction depends on the sample completeness, but also on the slope of the $R_e - \mu_e$ relation. This slope changes from approx. 0.33 in B and V, to 0.28 in I, to approx. 0.22 in H and K, reflecting the presence of a well defined color-magnitude relation among early-type galaxies. As a result, samples characterized by similar completeness can have significantly different corrections (compare, for example, the V and r band samples).

For the K band sample we compute two different completeness corrections. The first one is based on the results of the fit to the incomplete sample. We have noticed, however, how the K band photometric data span a reduced dynamic range with respect to data in all other bands (see section 4). This might be the reason for the somewhat discrepant μ_e coefficient that we obtain for the K band FP relation: while in all other bands the value of this coefficient is around 0.34, in agreement also with most of the results presented in the literature, in K band we obtain a value of 0.40.
Thus we compute a second completeness correction for the K band FP, forcing the μ_e coefficient in the simulations to assume a value of 0.34. This results in a slightly larger correction to the log σ coefficient, that becomes 1.77 instead of the 1.70 derived from the first, normal correction. A larger K band data-set is required to understand the origin of the discrepancy present in the current sample.

After the application of the completeness corrections, the wavelength dependence of the FP tilt is still visible, although the smooth monotonic trend observed before the corrections were applied has somewhat disappeared. If we parameterize the FP tilt in terms of a change of the M/L ratio of early-type galaxies, M/L $\sim L^{\beta}$, as customary, we can obtain the wavelength dependence of the parameter β, which is shown in Fig. 6. We remark that systematic uncertainties introduced by the adopted FP fitting technique result in an uncertainty on the absolute zero-point of the vertical scale in this plot. The scale itself is instead a lot more secure, due to the homogeneous treatment of the various data-sets.

5.4 Correlation of the FP residuals

The FP residuals in the various bands, measured as the deviation of the individual log R_e values from the best fitting FP relation, are plotted in Fig. 7 against the H band residuals. A high degree of correlation is clearly visible, with only few objects showing a different behavior at different wavelengths. Since the photometric measurements in different bands are entirely independent, the observed correlations can hardly be explained by photometric errors. This confirms the conclusion that photometric errors contribute a negligible fraction of the observed FP scatter (e.g. Jorgensen et al. 1996, Scodeggio 1997). Other measurement errors that could produce the correlations seen in Fig. 7 include errors on σ, erroneous assumptions on the distance of individual galaxies, or systematic deviations from the de Vaucouleurs $r^{1/4}$ profile used in the determination of r_e and μ_e. Distance errors can be easily excluded, as the range in log R_e residuals would correspond to a 'depth' of the sample of approximately 7000 km s^{-1}, comparable to the distance to the Coma cluster itself. Systematic deviations from the $r^{1/4}$ profile have been identified (Caon et al. 1993, Graham et al. 1996), but the use of a more general light profile model to derive r_e and μ_e does not result into a reduced scatter in the FP relation (Graham & Colless 1997b). Therefore it does not appear likely that this broken structural homology might be at the origin of the scatter in the FP. Velocity dispersion measurement errors are known to provide a significant contribution to the observed FP scatter, but this contribution is somewhat smaller than that of the intrinsic scatter (i.e. the scatter not accounted for by measurement uncertainties), which is estimated to be approximately 15 per cent (e.g. Jorgensen et al. 1996, Scodeggio 1997). If this conclusion is correct, then differences in the intrinsic galaxy properties must be at the origin of the FP scatter.

6 DISCUSSION AND CONCLUSIONS

We have shown that the tilt of the FP relation changes with wavelength, decreasing significantly as we go from the B to the K photometric band. This trend is visible both before and after completeness corrections are applied to the parameters of the FP, and it is certainly not an artifact introduced by those corrections. Their effect on the measured FP tilt is not negligible, however, and should not be ignored when discussing the amplitude of the tilt, and its possible origins. On average, the result of these corrections is to increase the log σ coefficient in the FP by 0.2, while leaving the μ_e coefficient unchanged. Thus a net decrease of the tilt is produced.

The absolute value of the tilt is still somewhat uncertain, though, because of persisting uncertainties on the fitting technique that should be used to derive the FP parameters. We have found differences in the log σ coefficient between 0.03 and 0.22, depending on the sample used, when using two different algorithms to fit the FP relation (the one described in section 5.1, and the one used by Scodeggio et al. (1997a), based on the average of the three linear fits that can be obtained considering in turn one parameter of the FP as the dependent variable, and the remaining two as the independent ones). It seems however unlikely that the tilt could be made to disappear just adopting a different fitting procedure, since the one used here appears to produce the steepest FP template among those presented in the literature, and still the minimum tilt observed at K band is significantly different from zero. We therefore conclude that a complete explanation of the tilt cannot be obtained without invoking some contribution from broken homology or stellar population effects. This is in agreement with previous results obtained by Pahre & Djorgovski (1997), and by Mobasher et al. (1997), although the net value we obtain for the tilt at all bands is significantly smaller than the one found in those two studies.

Two practical recipes for taking into account possible structural and dynamical non-homology have been presented by Graham & Colless (1997a), and by Busarello et al. (1997). The first is based on the use of a more general Sersic $r^{1/n}$ profile (Sersic 1968), instead of the commonly used de Vaucouleurs $r^{1/4}$ one, to describe the light distribution of elliptical galaxies, and on the computation of a global velocity dispersion from the observed central one. The second considers only dynamical non-homology, and is based on the computation of a global 'velocity', derived taking into account the total kinetic energy (rotation plus velocity dispersion) of a galaxy. The application of both methods to real FP data-sets resulted in a reduction of the observed FP tilt, the most significant one obtained when the galaxy specific kinetic energy is considered instead of the central velocity dispersion (see Busarello et al. 1997). Since only the latter quantity is available for most of the galaxies in our sample, it is impossible to apply this method here with sufficient accuracy. However, given the magnitude of the tilt reduction discussed by Busarello et al., it is likely that a fully corrected K band FP relation would result to have zero tilt. This would be in agreement with results obtained using stellar population synthesis models (Worthey 1994, Buzzoni 1995, Worthey, Trager & Faber 1996) that predict elliptical galaxies to have a constant M/L ratio at K band.

Assuming this to be the case, the wavelength dependence of the FP tilt finds a simple explanation in terms of one well known property of elliptical galaxies, namely the fact that they populate a well defined color-magnitude (CM) relation. If M/L is constant at K band, then it must be a function of the galaxy luminosity at a different band, to produce the CM relation. In particular, the slope of the CM relation defines the power index of the luminosity dependence of M/L. We have taken the V-K vs. V CM relations of Bower et al. (1992), and of Mobasher et al. (1997), to derive the expected M/L $\sim L^{\beta}$ relation in V band. These authors find a slope of 0.082 and 0.12, respectively, for the CM relation of Virgo and Coma E and S0 galaxies. Considering the average of these two values, we obtain an expected relation M/L $\sim L_V{}^{0.10}$, to compare with the results from our FP analysis. From the tilt in the V band FP we derive M/L $\sim L_V{}^{0.19}$.
However, in our FP analysis, the K band FP still shows some tilt, that is equivalent to a relation M/L $\sim L_V{}^{0.08}$ (or M/L $\sim L_V{}^{0.06}$ if we were to consider the modified completeness correction discussed in section 5.3). If we assume that broken homology corrections erase the K band FP tilt, and take advantage of the fact that these corrections should be wavelength-independent, then we can derive the V band power index as the difference between the observed V and K band indices, for a value of 0.11 (0.13 in the case of the modified completeness corrections to the K band FP). The good agreement between the slopes of the M/L $\sim L_V{}^{\beta}$ relation derived from the CM and the FP relation indicates that the wavelength dependence of the FP tilt is a manifestation of the CM relation, seen through the effective surface brightness instead of through total magnitudes. This should not be surprising, given the fact that the effective radius is approximately independent of wavelength. Therefore systematic changes in magnitude, at fixed R_e, must directly correspond to changes in μ_e. Any mechanism that could explain the CM relation, like the presence of a mass-metal content relation for early-type galaxies (Arimoto & Yoshii 1987), will then explain also the presence of a wavelength dependent tilt in the FP, without requiring extreme variations in the age or metal content of early-type galaxies of the kind considered by Pahre & Djorgovski (1997). This result is in good agreement with the findings of Mobasher et al. (1997), obtained comparing the tilt of the FP relation at V and K band.

An obvious future extension of the present work is along the line traced by Burstein et al. (1997), who determined the properties of the "generalized" B band FP for a large number of gravitationally bound systems, spanning from globular clusters to groups and clusters of galaxies. As already pointed out by these authors, the use of the B band to compare the properties of early- and late-type galaxies has important limitations, and one would like to view the properties of these stellar systems in redder passbands less affected by dust and recent star formation. With the completion of the H band survey of early-type galaxies in the Coma Supercluster (of which the observations reported here are a subset), we are now in the position of accomplishing such a task, having obtained H band imaging observations for 950 galaxies in the direction of the Coma and Virgo clusters. Although spectroscopic observations (including velocity dispersion and HI or Hα rotation measurements) are available for little over 50 per cent of these galaxies, there will be enough material for attempting a multi-wavelength study of the generalized FP plane of early- and late-type galaxies.

ACKNOWLEDGMENTS

We are grateful to the TAC of the TIRGO Observatory for the generous time allocation to this project. We thank C. Baffa, A. Borriello, V. Calamai, B. Catinella, I. Randone, P. Ranfagni, M. Sozzi, P. Strambio for assistance during the observations. A special thank to V. Gavriusev for software assistance. MS wishes to thank Martha Haynes for her assistance on using the GALPHOT package, and Riccardo Giovanelli, Martha Haynes, Alvio Renzini, Cesare Chiosi, and Giuseppe Longo for useful discussions.

REFERENCES

Arimoto N., Yoshii Y., 1987, A&A, 173, 23
Biviano A., Durret F., Gerbal, D. Lefevre, O. Lobo, C. Mazure A. Slezak, E., 1995, A&A, 297, 610
Bower R., Lucey J., Ellis R., 1992, MNRAS, 254, 601
Burstein D., Davies R., Dressler A., Faber S., Remington P., Lynden-Bell D., Terlevich R., Wegner G., 1987, ApJS, 64, 601
Burstein D, Bender R., Faber S., Nolthenius R., 1997, AJ, 114, 1365
Busarello G., Capaccioli M., Capozziello S., Longo G., Puddu E., 1997, A&A, 320, 415
Buzzoni A., 1995, ApJS, 98, 69
Caon N., Capaccioli M., D'Onofrio M., 1993, MNRAS, 265, 1013
Ciotti L., Lanzoni B., Renzini A., 1996, MNRAS, 282, 1
Davies R., Burstein D., Dressler A., Faber S., Lynden-Bell D., Terlevich R., Wegner G., 1987, ApJS, 64, 581
de Carvalho R., Djorgovski G., 1989, ApJ, 341, L37
de Vaucouleurs G. 1948, Ann. Astrophys., 11, 247
de Vaucouleurs G., de Vaucouleurs, A., Corwin, H., Buta, R., Paturel, G., & Fouque, P., 1991, "Third Reference Catalogue of Bright Galaxies" New York: Springer) (RC3)
Djorgovski G., Davis M., 1987, ApJ, 313, 59
Djorgovski G., Santiago B., 1993, in ESO/EIPC workshop on Structure, Dynamics and Chemical Evolution of Early-type Galaxies, eds. J. Danziger et al., p. 59
D'Onofrio M., Capaccioli M., Zaggia S., Caon N., 1997, MNRAS, 289, 847
Dressler A., Lynden-Bell D., Burstein D., Davies R., Faber S., Terlevich R., Wegner G., 1987, ApJ, 313, 42
Dressler A., 1980, APJS, 42, 565
Dressler A., 1987, ApJ, 317, 1
Efron B. 1987, Journal Am. Stat. Assoc., 82, 171
Elias J., Frogel J., Matthews K., Neugebauer G., 1982, AJ, 87, 1029
Faber S., Wegner G., Burstein D., Davies R., Dressler A., Lynden-Bell D., Terlevich R., 1989, ApJS, 69, 763
Gavazzi G., 1987, ApJ, 320, 96
Gavazzi G., Randone I., Branchini E., 1995, ApJ, 438, 590
Gavazzi G., Pierini D., Baffa C., Lisi F., Hunt L., Boselli A., 1996, A&AS, 120, 521.
Giovanelli R., Haynes M., Herter T., Vogt N., da Costa L., Freudling W., Salzer J., Wegner G., 1997, AJ, 113, 53
Graham A., Colless M., 1997a, MNRAS, 287, 221
Graham A., Colless M., 1997b, in Dark and Visible Matter in Galaxies, ASP Conf. Series 117, eds. M. Persic and P. Salucci, p. 172.
Graham A., Lauer T., Colless M., Postman M., 1996, ApJ, 465, 534
Guzmàn R., Lucey J., Bower R., 1993, MNRAS, 256, 731
Jørgensen I., Franx M., Kjærgaard P., 1995, MNRAS, 273, 1097
Jørgensen I., Franx M., Kjærgaard P., 1996, MNRAS, 280, 167
Hjorth J., Madsen J., 1995, ApJ, 445, 55
Kogut A., et al. 1993, ApJ, 419, 1
Kormendy J., 1977, ApJ, 218, 333
Lisi F., Baffa C., Hunt L., 1993, SPIE, 1495, 594
Lisi F., et al. 1996, PASP, 108, 364
Lucey J., Bower R., Ellis R., 1991a, MNRAS, 249, 755
Lucey J., Guzmàn R., Carter D., Terlevich R., 1991b, MNRAS, 253, 584
Mobasher B., Guzmàn R., Argon-Salamanca A., Zepf S., 1997, astro-ph/9703089
Pahre M., Djorgovski G., 1997, in The Nature of Elliptical Galaxies, Proceedings of the Second Stromlo Symposium, ASP Conf. Series 116, eds. M. Arnaboldi, G. S. Da Costa, and P. Saha, p. 154
Pahre M., Djorgovski G., de Carvalho R., 1995, ApJ, 453, L17
Press W.H., Teukolsky S., Vetterling W., Flannery, B., 1992, Numerical Recipes, 2nd edition (Cambridge: Cambridge University Press)
Prugliel P., Simien F., 1996, A&A, 309, 749
Renzini A., Ciotti L., 1993, ApJ, 416, L49
Saglia R., Bender R., Dressler A., 1993a, A&A, 279, 75
Saglia R., Bertschinger E., Baggley G., Burstein D., Colless M., Davies R., McMahan R., Wegner G., 1993b, MNRAS, 264, 961
Sandage A., 1994a, ApJ, 430, 1
Sandage A., 1994b, ApJ, 430, 13
Sandage A., Binggeli B., Tammann G., 1985, AJ, 90, 1759
Sandage A., Tammann G., Federspiel M., 1995, ApJ, 452, 1
Scodeggio M., 1997, PhD Thesis, Cornell University
Scodeggio M., Giovanelli R., Haynes M., 1997a, AJ, 113, 101
Scodeggio M., Giovanelli R., Haynes M., 1997b, AJ, 113, 2087
Scodeggio M., Giovanelli R., Haynes M., 1998a, submitted to AJ
Scodeggio M., et al. 1998b, in preparation
Sersic J.-L., 1968, Atlas de Galaxias Australes (Cordoba: Observatorio Astronomico)
Tukey J., 1958, Ann. Math. Stat., 29, 614
Teerikorpi P., 1987, A&A, 173, 39
Teerikorpi P., 1990, A&A, 234, 1
Thompson L., Gregory S., 1993, AJ, 106, 2197
Willick J., 1994, ApJS, 92, 1
Worthey G., 1994, ApJS, 95, 107
Worthey G., Trager S., Faber S., 1996, in Fresh Views of Elliptical Galaxies, ASP Conf. Series 86, eds. A. Buzzoni and A. Renzini, p. 203
Zwicky F., Herzog E., Karpoviwicz M., Kowal C., Wild P., 1961-68, Catalogue of Galaxies and Clusters of Galaxies (Pasadena: California Institute of Technology)(CGCG)

Table 1. FP parameters of Coma galaxies from the literature

band	A	B	b B/(-2.5)	β (2-A)/(2+A)	fit	ref
B	1.33	-0.83	0.33	0.20	LS	Dressler 1987
B	1.39	-0.90	0.36	0.18	S2F	Djorgovski & Davis 1987
V	1.23	-0.82	0.33	0.23	LS	Lucey et al. 1991a
r	1.24	-0.82	0.33	0.23	OF	Jorgensen et al. 1996
I	1.25	-0.78	0.32	0.20	AV3LS	Scodeggio et al. 1997a
I	1.55	-0.81	0.32	0.13	ML	Scodeggio 1997d
k'	1.44	-0.79	0.32	0.16	BLS	Pahre et al. 1995
k'	1.66	-0.75	0.30	0.09	BLS	Pahre & Djorgovski 1997
K	1.22	-0.76	0.25	0.24	S3F	Mobasher et al. 1997
Virial	2	-1.0	0.4	0.0		

LS: Least-Squares
S2F: Symultaneous two-variable Fit
OF: Orthogonal Fit
AV3LS: Average of 3 Least-Squares
ML: Maximum Likelihood
BLS: Bivariate Least-Squares
S3F: Symultaneous three-variable Fit

Table 2. H band photometric parameters

CGCG (1)	r_e arcsec (2)	r_{ecorr} arcsec (3)	± arcsec (4)	logR_e kpc (5)	± kpc (6)	μ_e mag arcsec^{-2} (7)	μ_{ecorr} mag arcsec^{-2} (8)	± mag arcsec^{-2} (9)	seeing arcsec (10)
159089	6.62	6.34	0.59	0.470	0.039	16.95	16.79	0.12	2.0
160013	32.91	32.87	1.60	1.185	0.021	18.79	18.64	0.05	2.2
160017	8.03	7.53	0.99	0.545	0.054	16.76	16.60	0.18	3.2
160019	4.00	3.54	0.36	0.217	0.039	15.40	15.17	0.13	2.2
160021	14.86	14.63	0.72	0.833	0.021	17.69	17.56	0.06	2.4
160022	9.74	9.38	0.68	0.640	0.030	17.14	17.00	0.09	2.7
160023	4.11	3.58	0.32	0.222	0.034	16.11	15.88	0.11	2.4
160024	11.26	10.88	1.34	0.704	0.052	17.57	17.41	0.15	3.0
160027	4.30	4.00	0.42	0.270	0.042	16.56	16.39	0.14	1.8
160028	10.51	10.28	0.70	0.680	0.029	17.01	16.85	0.09	2.2
160033	19.93	19.60	9.19	0.960	0.200	19.20	19.08	0.54	3.3
160037	2.93	2.25	0.36	0.020	0.053	15.16	14.78	0.19	2.4
160039	22.93	22.77	0.95	1.025	0.018	17.87	17.72	0.05	2.6
160042	6.74	6.32	0.48	0.469	0.031	16.48	16.32	0.10	2.7
160044 N	5.80	5.53	0.21	0.411	0.016	16.26	16.10	0.05	1.9
160044 S	13.63	13.48	0.47	0.798	0.015	17.13	17.00	0.04	1.9
160046	4.38	4.00	0.22	0.270	0.022	15.87	15.66	0.07	2.1
160049	2.39	1.60	0.54	-0.128	0.097	15.26	14.70	0.35	2.9
160062	21.74	21.61	2.61	1.003	0.052	19.17	19.03	0.14	2.2
160063	4.37	3.66	0.69	0.231	0.068	16.08	15.83	0.23	2.9
160065	4.39	3.68	0.62	0.234	0.061	16.13	15.86	0.20	2.9
160070	8.88	8.51	1.05	0.598	0.051	17.55	17.38	0.16	2.7
160071	9.94	9.53	1.00	0.647	0.044	17.11	16.95	0.13	3.0
160079	8.38	7.75	1.69	0.557	0.087	16.90	16.68	0.28	3.7
160091	10.17	9.91	0.69	0.664	0.029	17.30	17.14	0.09	2.3
160092	5.20	4.86	1.39	0.354	0.116	17.39	17.22	0.37	2.1
160094	9.56	9.26	1.26	0.634	0.057	17.14	16.98	0.17	2.4
160097	4.72	4.30	0.44	0.301	0.041	15.95	15.77	0.13	2.3
160099	10.83	10.40	1.00	0.685	0.040	16.72	16.56	0.12	3.2
160100	2.25	1.70	0.24	-0.102	0.045	15.22	14.81	0.16	1.9
160103	7.68	7.25	0.98	0.528	0.055	16.33	16.14	0.18	2.9
160105	7.88	7.65	0.73	0.552	0.040	16.57	16.41	0.13	1.9
160113	7.69	7.37	0.85	0.535	0.048	17.17	17.03	0.15	2.3
160118	10.80	10.61	0.84	0.694	0.034	16.58	16.47	0.10	1.9
160123	3.70	3.11	0.65	0.161	0.076	16.10	15.85	0.26	2.4
160124	32.00	31.84	2.23	1.171	0.030	18.24	18.11	0.08	2.9
160130	20.17	20.03	0.84	0.970	0.018	18.04	17.90	0.05	2.3
160211	2.85	1.87	0.34	-0.060	0.051	15.43	14.87	0.18	3.7
160215	6.85	6.69	0.21	0.493	0.013	16.51	16.35	0.04	1.5
160216	17.79	17.52	2.87	0.911	0.070	18.65	18.50	0.19	2.9
160217	3.00	2.16	0.51	0.002	0.074	15.85	15.39	0.26	2.9
160218	3.68	2.88	0.60	0.127	0.071	15.53	15.18	0.25	2.9
160219	4.33	3.61	0.63	0.225	0.063	16.33	16.07	0.21	2.9
160220	13.16	12.85	3.17	0.777	0.105	18.54	18.40	0.30	2.9
160221	6.33	5.89	0.36	0.438	0.025	16.54	16.36	0.08	2.7
160222	4.98	4.43	0.81	0.314	0.071	16.35	16.17	0.23	2.7
160224	8.09	7.71	0.50	0.555	0.027	16.36	16.24	0.09	2.7
160227	11.72	11.54	0.80	0.730	0.030	17.84	17.70	0.08	1.9
160228	3.74	3.29	0.43	0.185	0.050	15.76	15.57	0.17	2.1
160229	10.15	9.95	0.80	0.666	0.034	17.67	17.55	0.10	1.9
160230	3.03	2.57	0.27	0.078	0.038	15.46	15.20	0.13	1.9
160231	20.90	20.79	1.05	0.986	0.022	17.83	17.70	0.06	1.9
160234	7.30	6.85	0.83	0.504	0.049	16.97	16.80	0.15	2.9
160235	6.06	5.79	0.76	0.431	0.054	17.34	17.16	0.17	1.9
160237	8.18	7.89	0.79	0.565	0.042	17.26	17.08	0.13	2.2
160238	6.30	5.96	0.60	0.443	0.042	16.53	16.37	0.13	2.3
160239	12.43	12.28	1.01	0.757	0.035	18.26	18.13	0.10	1.8
160241	27.66	27.63	0.66	1.109	0.010	17.36	17.24	0.03	1.8
160242	4.78	4.48	0.51	0.319	0.046	17.02	16.83	0.14	1.9
160244	2.82	2.47	0.14	0.061	0.022	15.44	15.21	0.07	1.6
160246	2.72	2.13	0.44	-0.004	0.070	15.69	15.36	0.24	2.1
160247	21.84	21.69	4.56	1.004	0.091	19.47	19.39	0.24	2.4
160248 E	10.15	9.87	3.40	0.662	0.145	18.06	17.91	0.40	2.4
160248 W	6.02	5.64	0.52	0.419	0.037	16.12	15.95	0.12	2.4
160249	18.59	18.43	1.57	0.933	0.037	17.62	17.45	0.11	2.4
160250	6.09	5.79	0.64	0.431	0.045	17.21	17.02	0.14	2.1
160253	5.72	5.43	0.45	0.403	0.034	16.70	16.53	0.11	2.0
160254	12.22	11.94	2.52	0.745	0.090	18.32	18.18	0.26	2.6
160255 S	7.519	7.15	1.57	0.522	0.091	17.88	17.73	0.28	2.6
160255 N	3.87	3.22	0.81	0.176	0.091	15.89	15.64	0.31	2.6
160256	5.74	5.35	0.66	0.396	0.050	16.16	15.98	0.16	2.4
160258	8.00	7.67	0.47	0.553	0.026	16.74	16.55	0.08	2.4
160259	15.81	15.60	0.72	0.861	0.020	17.95	17.85	0.06	2.4
160261	20.33	20.11	4.61	0.971	0.098	18.77	18.64	0.27	2.9

Table 3, printed in Landscape format, to go here.

Table 3.

Table 3, printed in Landscape format, to go here.

Table 3.

Table 3, printed in Landscape format, to go here.

Table 3.

Table 3, printed in Landscape format, to go here.

Table 3.

Table 4. Completeness Parameters

Band	B_{compl} mag	cut-off
B	14.30	0.60
V	14.50	0.70
r	14.45	0.80
I	15.30	0.60
H	15.35	0.45
K	14.20	0.45

Table 5. the derived FP parameters (incomplete)

Band	N	A	±	b	±	dispersion	β	±
B	38	1.13	0.08	0.35	0.02	0.06	0.28	0.027
V	41	1.18	0.13	0.35	0.02	0.07	0.26	0.042
r	54	1.23	0.08	0.36	0.02	0.08	0.24	0.025
I	75	1.36	0.12	0.32	0.01	0.08	0.18	0.036
H	73	1.51	0.09	0.32	0.01	0.09	0.14	0.026
K	29	1.54	0.17	0.40	0.04	0.07	0.13	0.048

Table 6. the derived FP parameters (complete)

Band	N	A	±	b	±	dispersion	β	±
B	38	1.40	0.09	0.35	0.02	0.07	0.18	0.027
V	41	1.35	0.13	0.35	0.02	0.07	0.19	0.040
r	54	1.35	0.09	0.37	0.02	0.08	0.19	0.027
I	75	1.70	0.13	0.33	0.01	0.09	0.08	0.035
H	73	1.66	0.10	0.34	0.01	0.09	0.09	0.027
K	29	1.70	0.17	0.41	0.05	0.07	0.08	0.046
K_{mod}	29	1.77	0.17	0.34	0.07		0.06	0.045

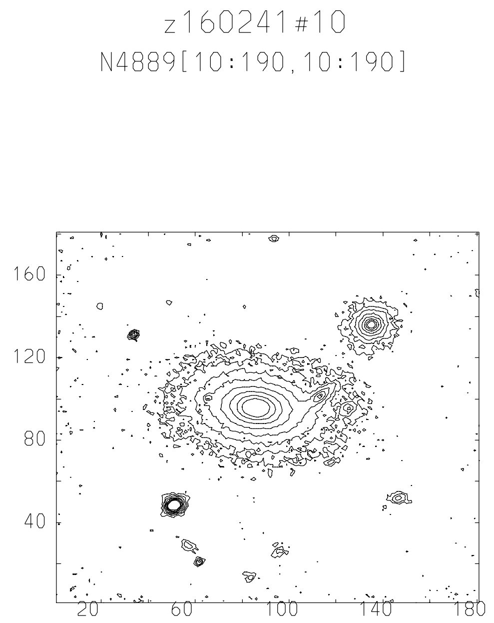

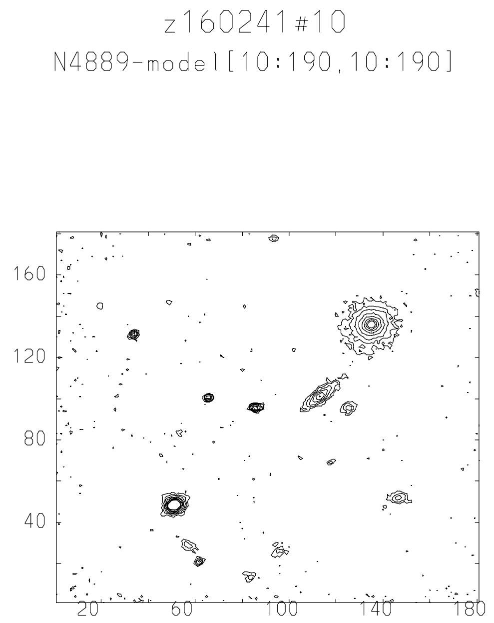

Figure 1. The H band frame of NGC 4889 (160241) prior (a) and after (b) subtraction of the model of the galaxy. The contour levels are from 19.5 to 16 $mag\ arcsec^{-2}$ in steps of 0.5. North is up and East to the left. The displayed frame is 3x3 arcmin^2.

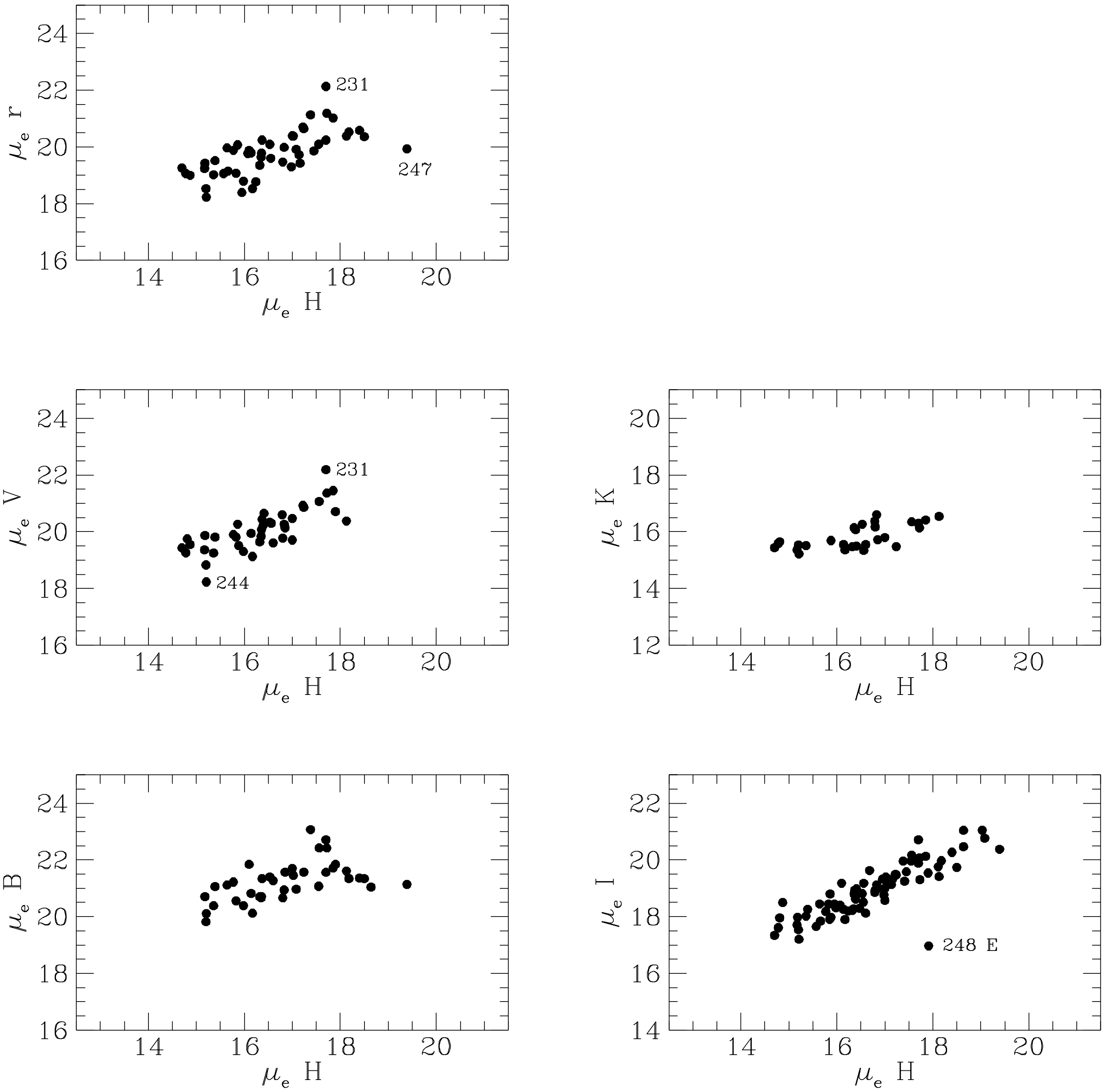

Figure 2. a) The relation between μ_e as derived in the various bands and μ_e in the H band. b) The relation between the effective metric radius as derived in the various bands and log R_e in the H band. Few discrepant galaxies are marked, using the last digits of their CGCG number. c) The relation between the values of the combination of μ_e and r_e that enters in the FP relation, when the two parameters are derived in the various bands and in the H band.

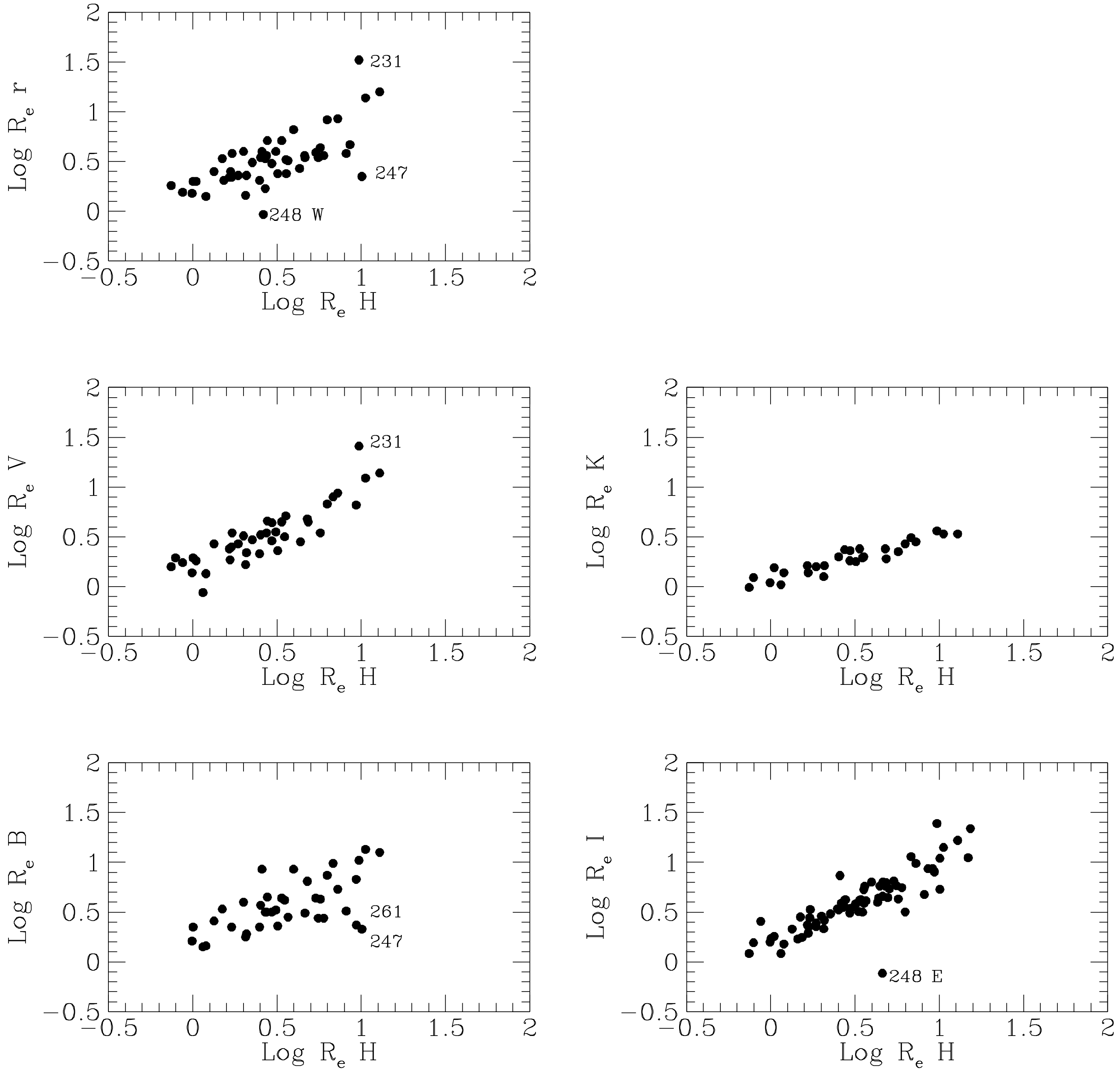

Figure 2. (Continued)

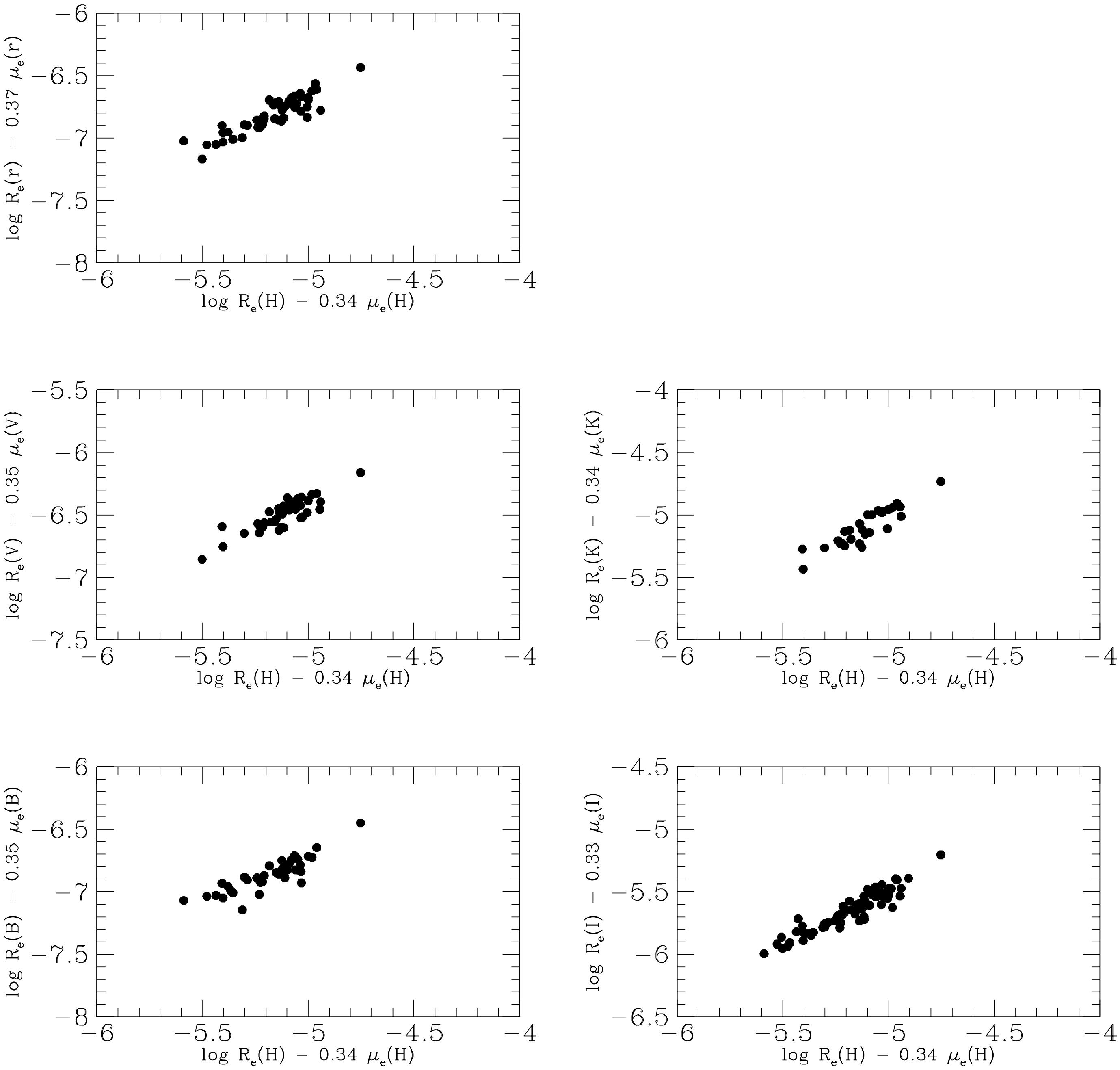

Figure 2. (Continued)

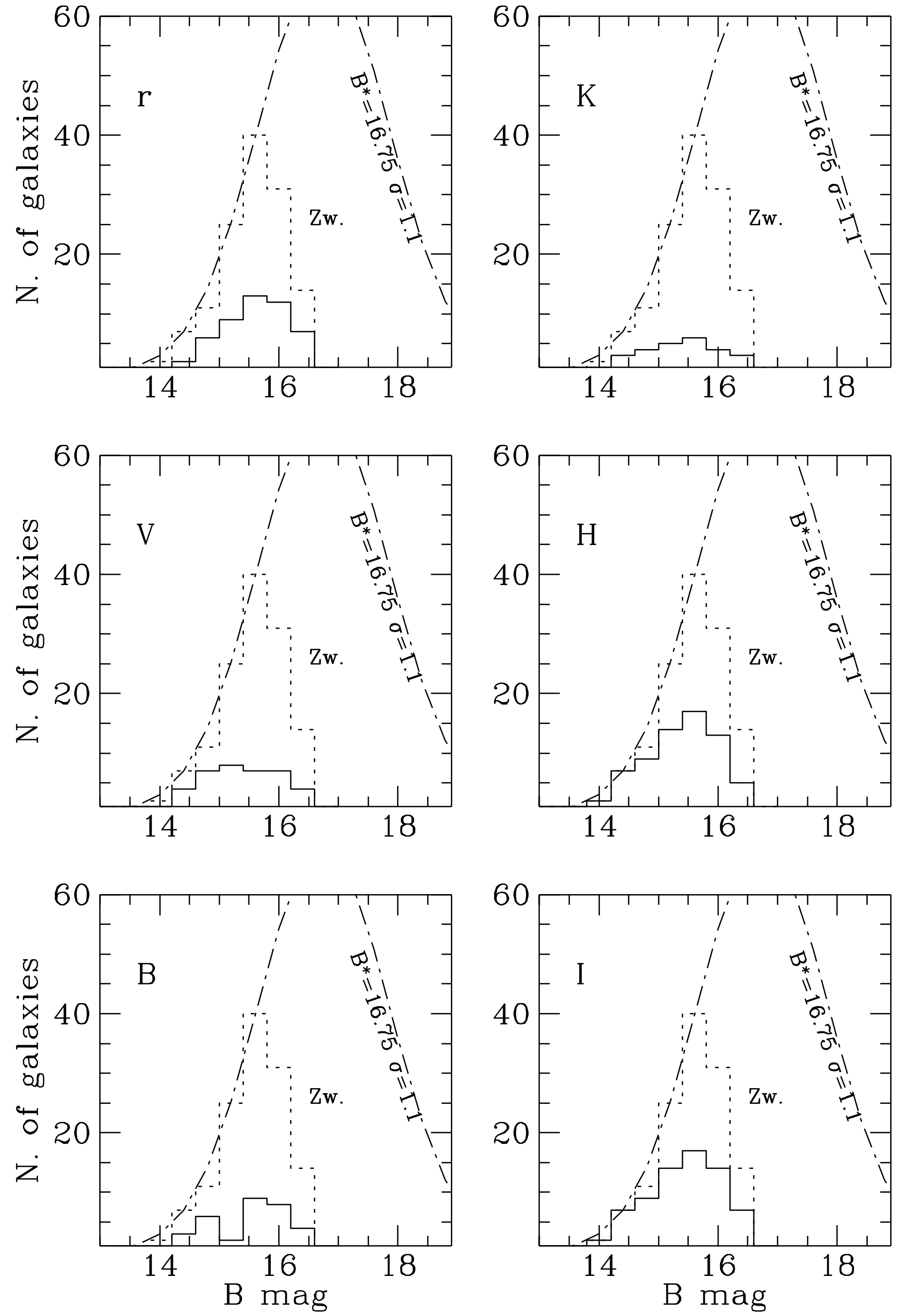

Figure 3. Apparent B mag distribution of Early-type Coma cluster galaxies in the various subsamples. The solid histograms show the objects included in the FP study. The dotted histograms give the CGCG distribution. The dotted-dashed curve is the adopted Gaussian luminosity function.

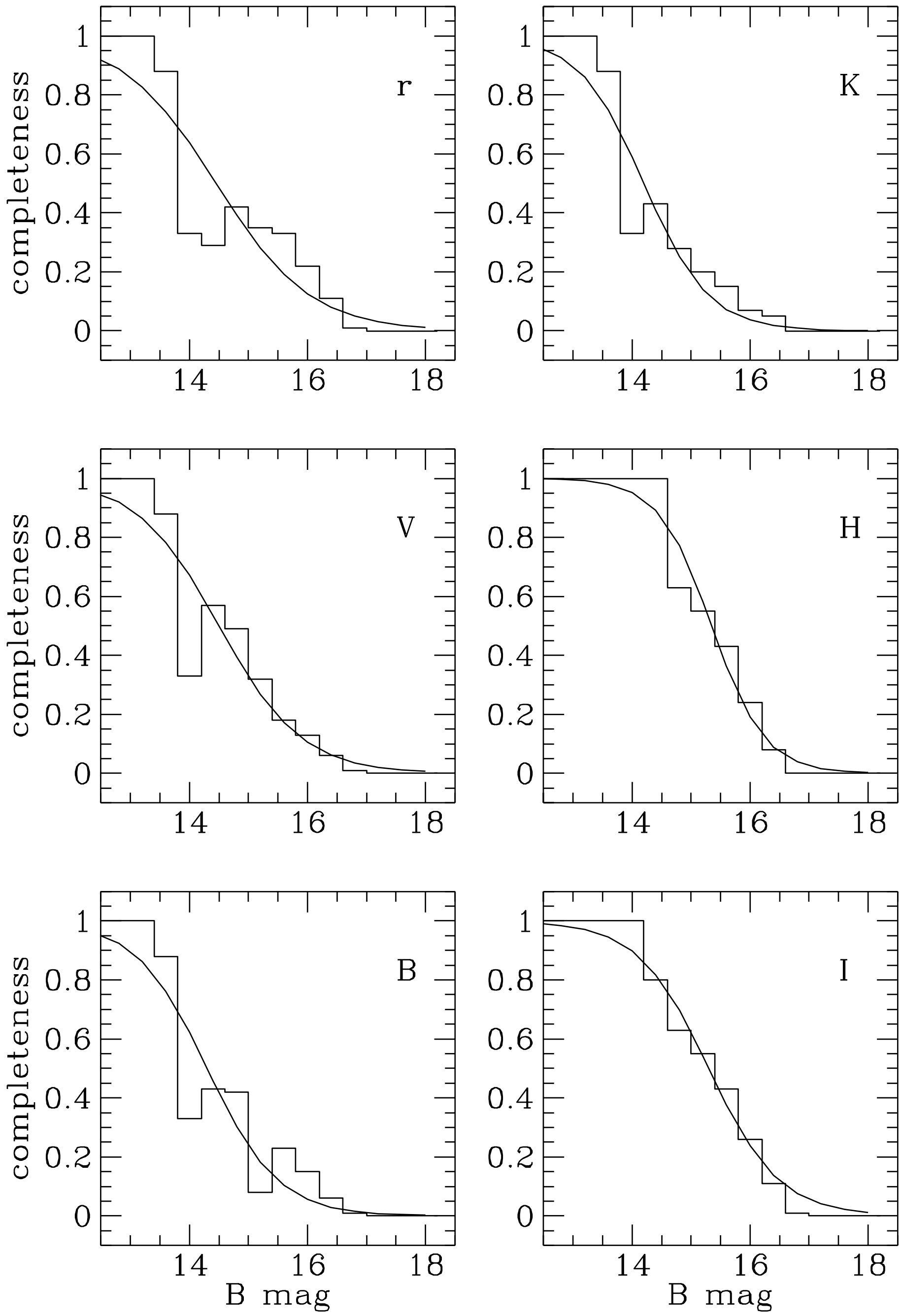

Figure 4. Completeness of the FP samples in the six bands. The histograms represent the ratio of the number of objects in each band used in the FP determination to the number predicted by the Gaussian luminosity function of Figure 3. The solid line is the best fit using a Fermi–Dirac function.

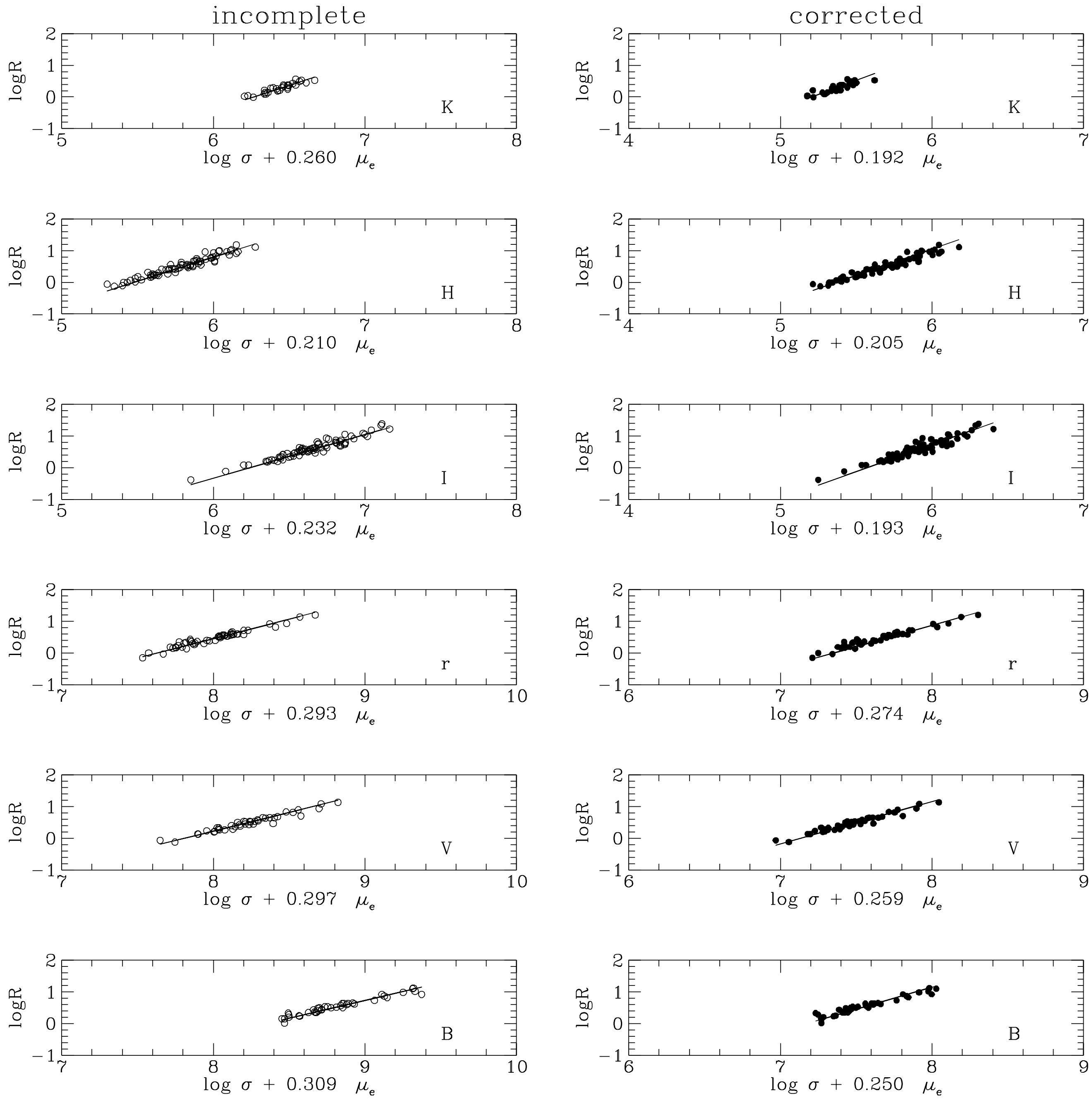

Figure 5. Edge-on view of the Fundamental Plane for the six studied bands. Left panels: before completeness corrections. Right panels: after completeness correction. The solid line represents the best fit FP parameters given in Table 5 and 6.

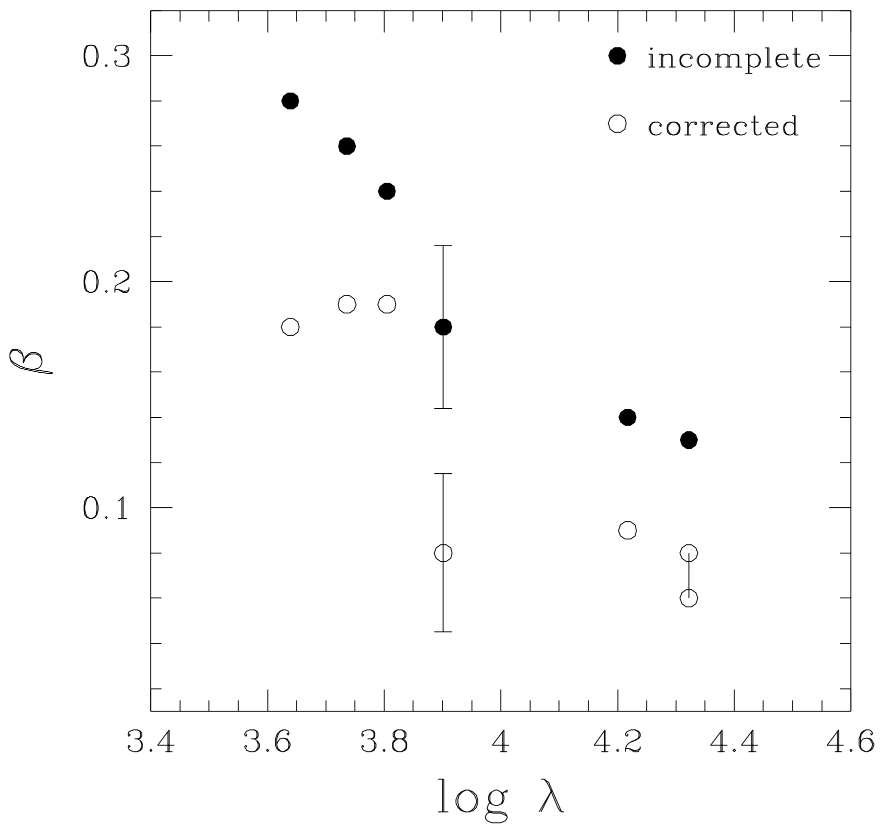

Figure 6. The dependence of β on wavelength prior and after correction for completeness. Two values for the corrected β at K band are shown connected by a line (see text). Errorbars are shown only for one point, to avoid confusion in the plot. They are however representative of the average uncertainty with which each value of β is determined. Tables 5 and 6 list all individual values for these uncertainties.

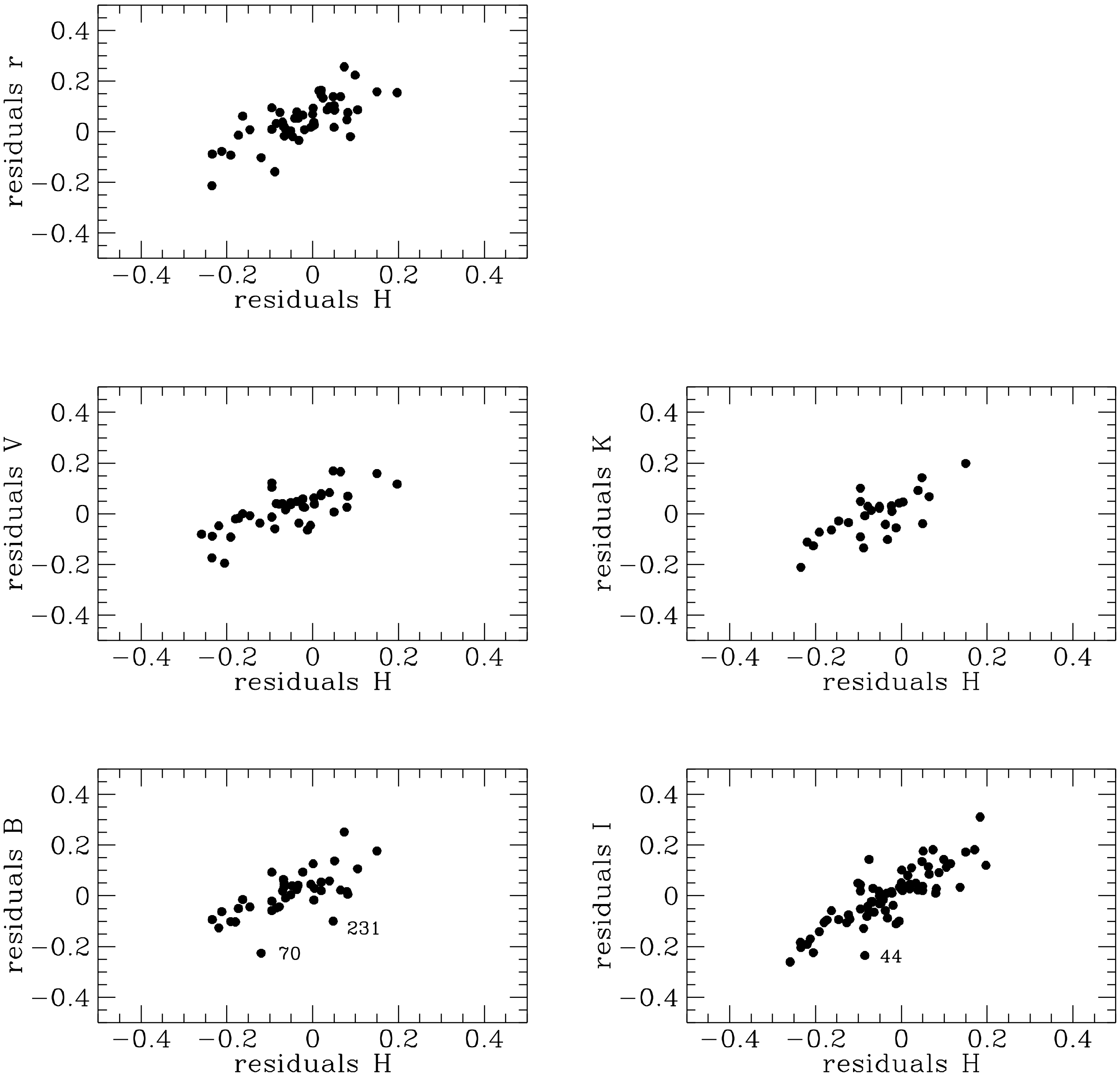

Figure 7. The relation between FP residuals (measured as the difference betwen the observed value of $\log R_e$ and the value predicted by the FP relation) in the various bands and the H band residuals. Few discrepant galaxies are marked, using the last digits of their CGCG number.